



**GPR vs. GEOARCHEOLOGICAL FINDINGS IN A COMPLEX
ARCHEOLOGICAL SITE (BADIA POZZEVERI, ITALY)**

Journal:	<i>Archaeological Prospection</i>
Manuscript ID	ARP-16-0011.R2
Wiley - Manuscript type:	Research Article
Date Submitted by the Author:	n/a
Complete List of Authors:	Ribolini, Adriano; University of Pisa, Department of Earth Sciences Bini, Monica; University of Pisa, Department of Earth Sciences Isola, Ilaria; Institut of Geophysics and Volcanology Coschino, Francesco; University of Pisa, Department of Translational Research on New Technologies in Medicine and Surgery, Division of Paleopathology Baroni, Carlo; University of Pisa, Department of Earth Sciences Salvatore, Maria Cristina; University of Pisa, Department of Earth Sciences Zanchetta, Giovanni; University of Pisa, Department of Earth Sciences Fornaciari, Antonio; University of Pisa, Department of Translational Research on New Technologies in Medicine and Surgery, Division of Paleopathology
Keywords:	Ground Penetrating Radar, GPR data processing, 12th century abbay, Italy, archaeological stratigraphy, GPR data interpretation

SCHOLARONE™
Manuscripts

1 GPR vs. GEOARCHEOLOGICAL FINDINGS IN A COMPLEX ARCHEOLOGICAL SITE
(BADIA POZZEVERI, ITALY)

RIBOLINI A., *Dipartimento di Scienze della Terra, University of Pisa, Italy*

BINI M., *Dipartimento di Scienze della Terra, University of Pisa, Italy*

ISOLA I., *Istituto di Geofisica e Vulcanologia, Pisa*

COSCHINO F., *Dipartimento di Ricerca Translazionale delle Nuove Tecnologie in Medicina e Chirurgia, Divisione di Paleopatologia, Università di Pisa, Italy*

BARONI C., *Dipartimento di Scienze della Terra, University of Pisa, Italy*

SALVATORE M.C., *Dipartimento di Scienze della Terra, University of Pisa, Italy*

ZANCHETTA G., *Dipartimento di Scienze della Terra, University of Pisa, Italy*

FORNACIARI A., *Division of Paleopathology, Department of Translational Research on New Technologies in Medicine and Surgery, University of Pisa.*

ABSTRACT

The results of a ground-penetrating radar (GPR) survey were compared with the archaeological excavation outcomes of a 12th century abbey site (Badia Pozzeveri). The goal was to associate the types of reflections recorded in GPR profiles and high-amplitude features visible in amplitude maps with unearthed archaeological features. GPR profiles crossing the walls evidenced axes of hyperbolic point source reflections and short planar reflections respectively generated by the stones forming the lateral sides/upper corners and the top of the structure. Moreover, the stones in the core of the wall caused small hyperbolic point source reflections with interfering axes, which produced a chaotic reflection profile. The resampling and gridding of these reflections collectively generated high-amplitude linear features in the amplitude maps. The presence in the graves of bones generates small hyperbolic point source reflections with interfering axes in the GPR profile, with a consequently chaotic reflection profile. Moreover, the existence of lythic slabs topping and/or siding the graves generates short planar reflections and axes of hyperbolic point source reflections. The resampling and gridding of these types of reflections generates in the amplitude map features that cannot be locally distinguished from those caused by the local aggregation of sediments with no archaeological relevance. The GPR profiles crossing trenches and pit-kiln showed dipping and concave upward reflectors unconformably resting on a basal planar reflector. Disconformity marks the onset of trench and pit-kiln decommissioning with the infilling of clayey silty layers and anthropogenic remains. These features in the amplitude maps correspond to medium to high-amplitude irregular areas.

The results show that types of reflection can be associated to specific elements of archaeological structure for a detailed interpretation of a complex subsurface setting. Furthermore, it is evidenced that the interpretation of GPR profiles must be considered an indispensable pre-requisite for a full comprehension of amplitude maps.

1. INTRODUCTION

The relationship between reflected ground-penetrating radar (GPR) waves and the electromagnetic nature of subsurface materials has been deeply explored in recent experiments, leading to more robust data inversion processes (Van Dam, 2000; Seung-Yeup *et al.*, 2007; Porsani *et al.*, 2010; Cataldo *et al.*, 2014). In the specific case of buried archaeological remains, laboratory experiments and numerical simulations have demonstrated the GPR potential and resolution limits due to the frequency and directionality of the antennas employed (Leckebush and Peikert, 2001; Goodman and Piro, 2014). Furthermore, the use of GPR with a multi-frequency antenna or an array of antennas has represented an important step forward in increasing image resolution and in maintaining an adequate investigation depth (Leckebush, 2003; Francese *et al.*, 2009; Novo *et al.*, 2012).

Despite these improvements, GPR data frequently suffer from interpretative complexity, which derives from the strong heterogeneity of most of the near-surface layers. In some archaeological sites, the overlap of time-variable structures composed of different materials, accumulations of building demolitions, anthropogenetic deposits, cavities, trenches, graves, and pedostratigraphic horizons complicate the interpretation of GPR images. Forward modeling experiments may be a valid help (Goodman and Piro, 2014), although subsurface complexity cannot always be represented in detail.

In this regard, validations of GPR interpretation by augering tests or visual comparisons from excavated sections are rare (Yalçiner *et al.*, 2009; Conyers, 2012; Conyers, 2015 and references therein), and an enrichment of GPR results linked to direct observations is necessary to consolidate schemes of interpretation.

The aim of this work is to illustrate the relationship between the results of a GPR survey in an archaeological area and the excavation outcomes. The relation between type of single GPR reflections, reflective patterns, and different archeological findings will be analyzed by a visual comparison of excavation surfaces, GPR profile, and amplitude map. The geo-stratigraphic context in which the archaeological settlement was developed will also be considered during data analysis.

The GPR data are related to several acquisitions from the archaeological site of “San Pietro di Pozzeveri” in the village of Badia Pozzeveri near Lucca. Archeological excavations were performed over the same areas that had been surveyed by GPR, outside the church of San Pietro. The interpretative procedures, calibrated and validated from the excavation results, were used for GPR data interpretation of the internal sector of the church, still unexcavated today.

2. DESCRIPTION OF THE SITE

1
2
3 81 This study focuses on the archaeological site of “San Pietro a Pozzeveri” in the village of
4 82 Badia Pozzeveri, located approximately 10 km southeast of the city of Lucca (NW Italy,
5 83 Fig. 1a).
6
7 84 The site and the village stand on Middle Pleistocene fluvial deposits, which are composed
8 85 of pebbles, sand, and clayey sands (Nardi *et al.*, 1997, Fig. 1b). These fluvial deposits
9 86 were terraced after the erosion phases that have started to affect the tectonic depression
10 87 of the Lucca plain since the Lower Pleistocene (Puccinelli, 1991). The most depressed
11 88 part of this basin was occupied by Lake Bientina (the former Lake of Sesto), the ancient
12 89 extension of which is marked by the outcrops of silty clay and locally peaty sediments (Fig.
13 90 1b).
14
15 91 The church of San Pietro was once part of a Camaldolese monastery, founded on the
16 92 shores of the Lake of Sesto in the 11th century (Figs. 2a, b, and c), on the site of a
17 93 medieval religious settlement formed by a church (documented in the year 1039) and a
18 94 “*canonica*” founded in the year 1056 (Fornaciari, 2014). The medieval lake, now entirely
19 95 dried up, underwent a complex evolution caused by changes in the fluvial dynamics of the
20 96 Serchio river (Nardi *et al.*, 1987), reaching a perimeter of 50 km during its maximum
21 97 extension when it was the largest lake in Tuscany (Federici, 1987). The monastery
22 98 flourished during the 12-13th centuries thanks to its location along the Via Francigena, a
23 99 major trade and pilgrimage route, which connected France and Northern Europe with
24 100 Rome throughout the entire Middle Ages. The decline of the monastery started in the 14th
25 101 century and eventually led to its dissolution in the 15th century. The church of San Pietro
26 102 remained as center of worship and is still in use today (Fornaciari, 2014). Although ancient
27 103 maps depict the monastery as being roughly as large as it is today (Fig. 2c), other
28 104 documents argue that it must have been more extended, in accordance with the religious
29 105 and economic importance of the site (Seghieri, 2006).
30 106 The archaeological excavation of the site has been performed by the University of Pisa
31 107 (Division of Paleopathology) and by Ohio State University (Department of Anthropology)
32 108 since 2011, in an attempt to reconstruct the architectural evolution of the monastery and to
33 109 obtain, by an intensive exploration of the graves, a large set of osteological samples for
34 110 bioarchaeological studies of the medieval and modern Tuscan population (Gibbons, 2013;
35 111 Fornaciari *et al.*, 2014; Fornaciari *et al.*, 2015).
36 112

37
38
39
40
41
42 113 3. METHODS
43 114

44
45
46 115 3.1 ARCHAEOLOGICAL EXCAVATION AND DOCUMENTATION
47 116

48
49 117 The archaeological excavation of the Badia Pozzeveri site was conducted by the “open
50 118 areas method”: three areas covering a total surface of 720 m² around the current church of
51 119 San Pietro were opened during the 2011-2015 archaeological campaigns to investigate
52 120 the presence of grave structures and to understand the developmental plan of the
53 121 medieval monastic buildings. The excavations were accompanied by constant
54 122 documentation via three-dimensional and GIS computer surveys, which allowed the
55 123 researchers to create a geodatabase containing all the archaeological, anthropological,
56 124 and topographic data.
57 125
58
59
60

3.2 GROUND PENETRATING RADAR

Ground-Penetrating Radar is widely used to image subsurface objects and stratigraphy, where relevant contrasts in the electro-magnetic (EM) properties among the media occur (Davis and Annan, 1989; Smith and Jol, 1995; Annan, 2009). Contrasts in the EM characteristics are reflected back to a receiving antennae (Rx) via the energy transferred into the soil by transmitting antennae (Tx). Significant advantages are possible by adopting a grid of radar profiles, which allow pseudo-3D imaging of the subsurface, where GPR data are interpolated to build a planar view at different depths (amplitude maps) (Goodman *et al.*, 1995; Malagodi *et al.*, 1996; Nuzzo *et al.*, 2002; Leckebush, 2003; Grasmueck *et al.*, 2004; Soldovieri and Orlando, 2009; Bini *et al.*, 2010; Novo *et al.*, 2012; Tinelli *et al.*, 2012).

The GPR survey was carried out at the archeological site following consistently oriented grids (Fig. 3). In particular, four sectors (one inside and three outside the church) were surveyed by GPR for a total area of more than 1000 m². A Radar System from the IDS Company© (www.ids-spa.it) equipped with a monostatic transmitter and receiver operating at 400 MHz (nominal peak frequency) via a shielded antennae was used. Moreover, to compare image resolution as a function of grid density and frequency, an array of seven monostatic 200 MHz antennas (STREAM X 200) was used in a survey sector also investigated with the 400 MHz single antenna (Fig. 3). The antenna array survey adopted 12 cm spaced parallel lines, whereas the single antenna survey adopted a grid of orthogonally spaced 50 cm lines. One of the directions of the 50 cm spaced grid was parallel to the antenna array acquisition direction (Fig. 3). The 400 MHz data were captured by continuous mode acquisition, checking the in-line trace spacing (2.4 m) with an odometer wheel. The configuration for acquisition provided 1024 samples/scan in a time window of 80 ns. The 200 MHz antenna array configuration provided 512 samples in a time window of 120 ns. An in-line trace spacing of 6 cm was adopted.

In both acquisitions, the spacing of GPR traces avoided spatial aliasing effects in the in-line direction. In the cross-line direction, the antenna channel separation of the STREAM X 200 array approached distances close to a quarter of the wavelength of the transmitted wavelength of the central antenna frequency, strongly limiting spatial aliasing effects (Novo *et al.*, 2012). Conversely, the characteristics of the 200 MHz antenna did not enable to reduce the cross-line distance, and spatial aliasing could be present.

A processing sequence was applied to the raw data following a standard procedure (Cassidy, 2009). The software GPR-Slice by Geophysical Archaeometry Laboratory Inc. was used for data processing and visualization. Specifically, a horizontal running average filter was applied to remove the saturation effect caused by Tx-Rx direct coupling. Subtraction of the mean trace from the dataset was performed to filter out continuous flat reflections caused by multiple reflections between the antenna and the ground surface. Following a spectral analysis of the measured signals, a band-pass filter was applied to the data to remove undesired frequency components coming from instrumental and environmental noises. Specifically, band pass filters with high/low cuts of 120-450 MHz and 80-350 MHz were tailored for the 400 and 200 MHz surveys, respectively. To enhance the visibility of deeper reflections due to signal attenuation, a linearly increasing in-depth gain function was applied to the data. In some sectors, the existence of diffraction

1
2
3 171 hyperbola scattered from a point source allowed the use of the synthetic hyperbola method
4 172 for EM wave velocity determination (Cassidy, 2009). The calculation in correspondence of
5 173 many hyperbolas provided a mean EM wave of 10 cm/ns, which was used for time-to-
6 174 depth migration at a constant velocity for the entire surveyed area. Such a defined flow
7 175 process was applied to each radargram.
8
9 176 The horizontal slicing of the 3D dataset was performed by stacking the absolute value of
10 177 EM energy in a time-window of 10 ns. This value was chosen as a function of the minimum
11 178 thickness of the majority of the expected archaeological findings, using the vertical
12 179 resolution at the given antenna frequency.
13
14 180 Data interpretation was initially performed by analyzing GPR profiles crossing different
15 181 types of archaeological findings, and then by analyzing the corresponding features in
16 182 amplitude maps.
17
18 183

19 184 4. RESULTS

20 185
21 186 4.1 OVERVIEW OF EXCAVATION STRUCTURES

22 187
23
24 188 The excavations made it possible to discover the foundations and portions of the elevated
25 189 structures of the abbey, as well as several medieval and modern grave features. In the
26 190 modern churchyard area, we discovered the foundation of the western portion of the
27 191 Camaldolensian abbey church (Fig. 4), which is 10 m longer than the modern church,
28 192 resized to the present dimensions in the 17th century. The sacred building of the 12th
29 193 century had a “Taucross plan” with an apse and a length of 34 meters. The structure
30 194 presented a 9 m wide nave and the transepts, which protruded from the body of the nave
31 195 for 5 m, were 7 m wide.
32
33 196 The walls found in the southern part of the churchyard presumably correspond to the
34 197 structures from a monastic building and were most likely developed around a
35 198 Romanesque cloister.
36
37 199 A structure, possibly an enclosure wall, was set up near the southwestern cantonal of the
38 200 church. It continued westward and probably circumscribed the monastic space intended
39 201 for the monks and *conversi*, but denied to the laity.
40
41 202 Privileged grave spaces for the monks were observed in what may have been the
42 203 ambulatory of the cloister, whereas the tombs of the prominent lay people contained lytic
43 204 coffins placed up against the N side of the nave and against the façade of the church.
44 205 Examples were also directly placed within the medieval churchyard. Other common lay
45 206 people were buried in simple ground trenches in the churchyard and in the area north of
46 207 the church (Fig 4). In three different sectors, traces of fusion activities linked to the
47 208 production of bells were unearthed. The first pit-kiln was found immediately NW of the
48 209 church and dates back to the late 18th century. A second pit-kiln dated to the 16th century
49 210 was identified in front of the present church. Another pit-kiln, dedicated to the same
50 211 function, but dating back to the 12-13th centuries, was detected further S, close to the
51 212 cloister of the monastery.
52
53 213 Finally, the excavation revealed a complex system of trench pipes for rainwater drainage
54 214 in the area of the modern churchyard. The largest drainage trench is contained in a funnel-
55 215 shaped section (2.5 m large on the surface and 0.8 m at the bottom) and originates near

the entrance of the church before proceeding W at a progressively increasing depth (Fig. 4).

4.2 GPR PROFILES VS. UNEARTHED ARCHAEOLOGICAL FINDINGS

The availability of excavation outcomes (Fig. 4) in the sectors where GPR surveys were made (Fig. 3) enables a visual correlation between selected GPR profiles and unearthed archaeological findings.

The excavation revealed that most of the walls were composed laterally by open-work decimeter sized boulders and internally by a core of smaller boulders sustained by abundant mortar. The GPR imaged the top of the structure as flat reflections, and the individual stones placed on the lateral sides and corners as axes of hyperbolic point source reflections (Fig. 5 a, c, e). The boulder in the mortar dominant core generated small hyperbolic reflections with interfering axes producing a chaotic radar profile (Figs. 5c).

It is possible to associate reflective features in the GPR profile to the graves. These features are: i) sub-horizontal reflections (Fig. 6a); ii) lateral truncation of reflections and one axis of hyperbolic point source reflections (Figs. 6b); and iii) small point source hyperbolic reflections with interfering axes (Fig. 6b, d). The first feature set may be associated with reflections from the material covering or flooring the grave (rock slabs and/or clayey sand layers bearing abundant cobbles). The second feature set is generated by the point source diffraction in correspondence of lateral interruptions of the sub-horizontal layers due to grave excavation. In addition, the same reflection type is generated by the side of the grave where it is composed by vertical rock slabs (Fig. 6c, e). The third feature set corresponds to the effect of diffractions from materials inside the graves, i.e., aggregates of sandy-clay matrix and bones (Figs. 6e, f). Locally, the presence of a partly void space inside the grave caused a polarity inversion of the GPR wave (see Fig. 6a between 9 and 10 m of horizontal distance). In the examined sectors, all these reflective features were detected both inside the excavated area and in the sectors not yet investigated, which means that the graves might have been placed not only near the main unearthed structures.

The existence of a drainage trench crossing the center of the modern churchyard (Fig. 4) was clearly imaged by the GPR. The hardened lateral edges of the trench generated two hyperbolic reflections. The sandy layers bearing small cobbles infilling the trench generated concave upward and horizontal reflections (Fig. 7a). Moreover, the coarse gravel and boulders with diameters on the decimeter scale found near the base of the trench (Fig. 7b) caused a reflection profile similar to the characteristics usually observed for a wall.

At the SW corner of sector 1, flat and slightly inclined reflectors show a clear angular unconformity with respect to a concave upward basal reflector (Figs. 7c, d, and e). These reflection types are consistent with the existence of a pit-kiln for lime production, as shown by the excavation results (Fig. 4 and 7f). The basal reflector is produced by a floor of lime layers corresponding to an initial phase of depression formation. The slightly inclined reflectors are caused by clayey silty layers interbedded with anthropogenic sediments (fragments of baked clay and charcoals), which were unconformably deposited on the base when the pit-kiln underwent decommissioning.

4.3 GPR Profiles vs. pedostratigraphy

The Badia Pozzeveri site stands on a Pleistocenic fluvial terrace composed of boulders, pebbles, sands, and clayey sands, affected by intense pedogenesis. The weathering profile may locally reach more than 1 m in depth. The GPR profiles exhibit a set of slightly inclined and sinuously shaped reflectors topped by flat reflectors (Fig. 8). These systematic truncations provide clear angular unconformities that are visible in the deepest part of the GPR section. These features in the radar profile are consistent with a layered fluvial deposit discordantly cut by erosive sub-horizontal surfaces. Apparent dips in the fluvial bedding are observed towards E. Wavy-shaped discontinuous reflectors are evident in the first 1-1.5 m of depth (Fig. 8). These reflectors mirror the pedogenetic layering, which is locally truncated by the archeological structures, i.e. the graves.

4.4 GPR AMPLITUDE MAPS

Amplitude maps were obtained for each sector by resampling and gridding the GPR profiles.

Sector 1 in front of the church is characterized by high-amplitude reflections, assuming a N-S and E-W alignment (A, B, C, D, E, L and I in Fig. 9a, b). It is noted that among the E-W linear reflections, the most external (D and I) correspond to the ideal prolongation of the walls of the nave of the church of San Pietro (Fig. 9c). The interior E-W reflection (L in Fig. 9b) above the aforementioned linear reflections originates from the present church entrance and continues outside the surveyed sector. The southernmost E-W reflection (E in Fig. 9a, b) also continues outside the surveyed sector.

Comparison of amplitude maps and map of archaeological findings, supported by individual GPR profiles, evidences that the N-S and E-W high-amplitude linear features correspond to the discovered walls. Moreover, the interior E-W linear amplitude feature (L in Fig 9b) corresponds to the base of the draining trench originated near the church entrance (see also Fig. 7a, b).

To the N-S and E-W alignments, an oblique high-amplitude linear reflection must be added, which from the corner of the church extends towards NW. This feature is generated by a modern pipe, as evidenced by the excavation and manhole on the surface.

Of particular importance are the presence of a high-amplitude reflection area of sub-squared shape in the NW corner (F in Fig. 9a, b) and an irregular high-amplitude reflection area near the SW corner (G in Fig. 9a). While the former falls within a non-excavated area, the latter corresponds to the unearthed pit-kiln already described (Fig. 7e, and f), whose lateral sides and infilling sediments have reflected back the EM energy.

Finally, the high-amplitude feature close to the church entrance (H in Fig. 9a) is consistent with the concentration of graves interred in the first decimeters of subsurface.

Sector 2, which is located on the southern side of the churchyard, exhibits a similar reflective pattern, with the high-amplitude linear features following the E-W and N-S linear directions (A, B, and C in Fig. 10a, b). The excavation outcomes (Fig. 4) and the GPR profiles confirmed that these linear features correspond to well preserved walls. Only in the

easternmost part is there evidence of a slightly oblique ENE-WSW-ENE linear reflection (D in Fig. 10a, b), which originated from a connection to a modern water conduit.

The reflective pattern from sector 3 on the northern side of the church exhibited more irregular characteristics than the previously mentioned sectors. The reflected energy in the first 20-30 cm below the surface is almost completely concentrated in the half sector nearest to the church (A in Fig. 11a). At the depths of 20-30 cm and 30-40 cm, some short and discontinuous linear amplitude features are visible, along with high-amplitude reflections locally delimiting sub-squared areas (B, C, D and E in Fig. 11b). The comparison with the maps of archaeological findings evidenced that the short and discontinuous linear amplitude features correspond to the alignment of graves (Fig. 4).

Sector 4, which is inside the church, clearly exhibits high-amplitude linear features crossing the central area of the church in the NS direction (A, B, C, F and G in Fig. 12a and b), which is visible up to a depth of 70-80 cm. Two EW high-amplitude linear features (D and E in Fig. 12a and b) are visible over a depth of 60-80 cm, one of which forms a right angle with a NS linear reflection. This sector was not excavated, but these high-amplitude linear features present the same reflective profile that corresponds to the unearthed walls in the external sectors.

4.5 MULTICHANNEL VS. SINGLE CHANNEL GPR

The W margin of sector 1 was also surveyed by using the multi-antenna GPR device (STREAM X, Fig. 3) at a nominal frequency of 200 MHz. The results confirm imaging from the 400 MHz single channel GPR. However, some differences can be observed by visual comparison (Fig. 13). STREAM X provides a better image of the N-S and E-W linear amplitude features at a depth of 40-50 cm (A, B, C in Fig. 13). Moreover, the irregular high-amplitude areas at the NW and SE corners (D and E in Fig. 13) result to be more delimited in the STREAM X data.

Below a depth of 80-90 cm, the results are similar for both datasets with the exception of the sub-rectangular high-amplitude area at the NW corner that is better defined in the STREAM X amplitude map (D in Fig. 13).

5. DISCUSSION

The comparison between archaeological findings and GPR profiles allowed to associate types of reflection with specific unearthed structures. This operation evidenced how, in most cases, walls, trench lateral sides and infilling sediments, graves and pit-kiln reflected back the EM energy producing detectable reflections. More specifically, it resulted evident that a careful examination of GPR profiles may enable to individuate single constitutive elements of an archaeological structure, i.e., side and top of a wall, grave cut and internal material, trench lateral sides and infilling sediments. However, the same type of reflection may be generated by constitutive elements of different archaeological structures, i.e., one axis point source hyperbolic reflection produced by the individual stone of the lateral side/corner of a wall and the edge of a grave cut. In this regard, the association of types of

1
2
3 351 reflections may support a correct interpretation. In the case of a wall, the apexes of point
4 352 source hyperbolic reflections from the opposite lateral sides may be located near a profile
5 353 area of flat an chaotic reflections, as produced by wall top and internal heterogeneities.
6
7 354 Trenches and pit-kiln were filled with sediments of various grain-size after their
8 355 decommissioning. The resulting layering generated reflections in the GPR profiles that can
9 356 be interpreted following the same concepts adopted to interpret those produced by a
10 357 natural (non cultural) stratigraphical setting. In this respect, angular discontinuities
11 358 indicate a change in the depositional setting, marking the onset of trench and pit-kiln
12 359 decommissioning.
13
14 360
15
16 361 The visual correlation between the amplitude maps and the map of archaeological findings
17 362 clearly shows positive matching between the linear amplitude features and the principal
18 363 walls. The mono and multichannel data substantially provided similar results, with a
19 364 geometrical coherence of the walls slightly higher in the STREAM X amplitude maps.
20 365 However, the amplitude maps failed to image the northernmost and southeasternmost
21 366 walls in sector 1 (see Figs. 9 and 4) and to provide a clear vision of the unearthed walls in
22 367 sector 3 (Figs 4 and 11). This failure in identifying the targets could be traced to the coarse
23 368 heterogeneous material in the nearby walls, which smooth the EM impedance contrast.
24 369 Indeed, in sector 3 the excavations revealed high concentrations of stones in the first
25 370 decimeters of subsurface coming from the demolishment of medieval buildings.
26 371 Additionally, the high density of 19th century graves (approximately 200 over an area of
27 372 less than 100 m²) generated several reflections in the profiles. When resampled and
28 373 gridded to build amplitude maps, such reflections altered the geometrical evidence of the
29 374 buried wall structures.
30
31 375 Amplitude maps clearly imaged the base of the drainage trench crossing the centre of
32 376 sector 1 (L in Fig. 9). In the map the evidence of the trench base is rather similar to that of
33 377 a wall, i.e. high amplitude linear reflection. However, the EM signal partition at the contact
34 378 between the trench flooring sediments (coarse gravel) and overlying material (sandy
35 379 layers) generated a reflection with an inverted polarity with respect to that of a wall
36 380 (compare Figs. 7a and 5a, c and e). The operation used to stack the absolute value of EM
37 381 energy for amplitude map generation operates on the reflection phase, making the trench
38 382 response similar to that of a wall. To avoid a misleading interpretation, the reflection phase
39 383 should be observed in the GPR profile.
40
41 384 With regard to graves, it is evident that, unlike the GPR profile, features within the
42 385 amplitude maps are not clearly distinguishable from reflections with no archaeological
43 386 relevance, i.e., concentration of pebbles/boulders. Although it may be argued that a
44 387 smaller separation between the acquisition lines would provide a more defined imaging,
45 388 the area investigated by the STREAM X system did not yield a better image of the
46 389 subsurface in terms of grave visibility. There are more than one possible explanations for
47 390 this mismatch. Grave material may have the same possibility of retaining humidity as local
48 391 sediment agglomerates, which provide the same response in the amplitude maps. On the
49 392 basis of cover, lateral rocky slabs, quantity of bones and characteristics of the basal layer,
50 393 the GPR profile records various types of reflective events. These reflections may interact
51 394 with each other, so that the final features may be rather irregular when sliced to form the
52 395 amplitude map.
53
54
55
56
57
58
59
60

6. CONCLUSIONS

Comparison of the GPR investigation results with subsequent excavation outcomes provided an insightful possibility to examine the effectiveness of GPR data capture strategies and processing sequences, and to consolidate interpretation choices.

The excavation results evidenced the existence of a complex archaeological setting, where the walls of different ages coexist with trenches, pit-kilns and a high concentration of graves. The interception of GPR profiles with single excavation outcomes made it possible to associate GPR reflection types with specific archaeological findings. This operation evidenced how, in most cases, walls, trenches, graves and pit-kilns produced reflection types coherent with their constitutive elements and layering of infilling sediments. The amplitude maps showed high-amplitude features consistent with the existence of walls and of a trench in the churchyard of the abbey site. The images were not satisfactory only when the archeological and natural material enclosing the wall and infilling the trenches had similar grain-size, state of aggregation, or capacity to retain water.

The several graves resulted more evident in the GPR profile than in the amplitude maps generated by both the mono- and multi-multichannel survey. The resampling and gridding of the different types of reflections caused by the constitutive elements of the graves (cover, floor, lateral slabs or internal material) generated irregular features in the amplitude map. These features were locally undistinguishable from those caused by concentrations of pebbles/boulders with no archaeological relevance.

The results highlight how a strict association of different types of reflection visible in the GPR profile with constitutive elements of archaeological structures is possible. Distinguishing between different types of reflections and looking at their association enables a detailed interpretation of a complex subsurface setting. Moreover, it resulted evident that the interpretation of GPR profiles must be considered an indispensable prerequisite for a full comprehension of amplitude maps. The amplitude maps may provide results that are well consistent with the principal structures, but unsatisfactory in imaging sectors with a high density of archaeological features, where the interference of different reflection types can be misinterpreted.

1
2
3
4
5
6
7
8
9
10
11
12
13
14
15
16
17
18
19
20
21
22
23
24
25
26
27
28
29
30
31
32
33
34
35
36
37
38
39
40
41
42
43
44
45
46
47
48
49
50
51
52
53
54
55
56
57
58
59
60

Acknowledgments:

This work was funded by the CA.RI.LU grant (2012-13): "New high resolution Georadar techniques for archeological contexts analysis" (Leader. A. Ribolini). We wish to thank Alex Novo for his useful suggestions about GPR-Slice data processing. The precious suggestions and comments by Lawrence Conyers and two anonymous reviewers highly improved the original version of the paper.

For Peer Review Only

References

- Annan, A.P., 2009. Electromagnetic principles of ground penetrating radar. In: Jol, H.M. (Ed.), *Ground Penetrating Radar: Theory and Applications*. Elsevier, pp. 3-40.
- Bini M., Fornaciari A., Ribolini A., Bianchi A., Sartini S., Coschino F. 2010. Medieval phases of settlement at Benabbio castle, Apennine mountains, Italy: evidence from ground penetrating radar survey. *Journal of Archaeological Sciences* **37**: 3059-3067.
- Cassidy N.J., 2009. Ground Penetrating Radar Data Processing, Modelling and Analysis. In: Jol H.M. (Ed.), *Ground Penetrating Radar: Theory and Applications*. Elsevier, pp. 141-176.
- Cataldo A., Persico R., Leucci G., De Benedetto E., Cannazza G., Matera L., De Giorgi L. 2014. Time domain reflectometry, ground penetrating radar and electrical resistivity tomography: A comparative analysis of alternative approaches for leak detection in underground pipes. *NDT&E International* **62**: 14-28
- Conyers L.B., 2012. *Interpreting Ground-Penetrating Radar for Archaeology*. Left Coast Press Inc., 220 pp.
- Conyers L.B., 2015. Analysis and interpretation of GPR datasets for integrated archaeological mapping. *Near Surface Geophysics* **13**: 645-651
- Damiata B., Steinberg J.M., Bolender J.D., Zoëga G. 2013. Imaging skeletal remains with ground-penetrating radar: comparative results over two graves from Viking Age and Medieval churchyards on the Stóra-Seyla farm, northern Iceland. *Journal of Archaeological Science* **40**: 268-278.
- Davis J.L., Annan A.P. 1989. Ground Penetrating Radar for high resolution mapping of soil and rock stratigraphy. *Geophysical Prospecting* **37**: 531-551.
- Federici P.R., 1987. Il territorio del Bientina: dalla geologia alla storia. in: *Il padule di Bientina-aspetti naturalistici ed agronomici*. Pacini, Pisa, 27-54.
- Fornaciari A. 2014. *Badia Pozzeveri. Dalla terra alla storia*. LUK 20, 30-36.
- Fornaciari A., Coschino F., Cariboni A., Cavallini L., Farnocchia A., Testi S. 2014. Badia Pozzeveri, Altopascio (LU). Terza campagna di scavo presso l'abbazia camaldolese di San Pietro (concessione di scavo). *Notiziario della Soprintendenza Archeologica della Toscana* **9/2013**: 191-196.
- Fornaciari A., Coschino F., Cariboni A., Cavallini L., Farnocchia A., Testi S. 2015. Altopascio (Lu). Badia Pozzeveri: quarta campagna di scavo presso l'abbazia camaldolese di San Pietro (concessione di scavo). *Notiziario della Soprintendenza Archeologica della Toscana* **10/2014**: 2015, in press.
- Francesse R.G., Finzi E., Morelli G. 2009. 3-D high-resolution multi-channel radar investigation of a Roman village in Northern Italy. *Journal of Applied Geophysics* **67**: 44-51.
- Gibbons A. 2013. The Thousand-Year Graveyard. *Science Magazine* **342**: 1306-1310.
- Goodman D., Nishimura Y., Rogers J.D. 1995. GPR time slices in archaeological prospection. *Archaeological Prospection* **2**: 85-89.
- Goodman D., Piro S., 2014. *GPR Remote Sensing in Archaeology*. Springer-Verlag, 233 pp.

- Grasmueck M., Weger R., Horstmeyer H. 2004. Three-dimensional ground-penetrating radar imaging of sedimentary structures, fractures, and archaeological features at submeter resolution. *Geology* **32**: 933-936.
- Yalçiner C.Ç., Bano M., Kadioglu M., Karabacak V., Meghraoui M., Altunel E. 2009. New temple discovery at the archaeological site of Nysa (western Turkey) using GPR method. *Journal of Archaeological Science* **36**: 1680-1689.
- Seung-Yeup H., Yu-Sun J., Heon-Cheol O., Se-Yun K., Young-Sik K. 2007. The laboratory scaled-down model of a ground-penetrating radar for leak detection of water pipes. *Measurement Science and Technology* **18**: 2791-2799. DOI:1088/0957-0233/18/9/008
- Smith D.G., Jol H.M. 1995. Ground penetrating radar: antenna frequencies and maximum probable depths of penetration in quaternary sediments. *Journal of Applied Geophysics* **33**: 93-100.
- Leckebush J. 2003. Ground-penetrating radar: A modern three-dimensional prospection method. *Archaeological Prospection* **10**: 213-240.
- Leckebush J., Peikert R. 2001. Investigating the True Resolution and Three-dimensional Capabilities of Ground-penetrating Radar Data in Archaeological Surveys: Measurements in a Sand Box. *Archaeological Prospection* **8**: 29-40.
- Malagodi S., Orlando L., Piro S., Rosso F. 1996. Location of archaeological structures using GPR method: three-dimensional data acquisition and radar signal processing. *Archaeological Prospection* **3**: 13-23.
- Nardi R., Nolledi G., Rossi F. 1997. Geologia e idrogeologia della pianura di Lucca. *Geografia Fisica e Dinamica Quaternaria* **10**: 132-160.
- Novo A., Dabas M., Morelli G. 2012. The STREAM X Multichannel GPR System: First Test at Vieil-Evreux (France) and Comparison with Other Geophysical Data. *Archaeological Prospection* **19**: 179-189.
- Nuzzo L., Leucci G., Negri S., Carrozzo M. T., Quarta, T. 2002. Application of 3D visualization techniques in the analysis of GPR data for archaeology. *Annals of Geophysics* **45**: 321-337.
- Porsani J.L., Slob E., Lima R.S., Leite D.N. 2010. Comparing detecting and location performance of perpendicular and parallel broadside GPR antenna orientations. *Journal of Applied Geophysics* **70**: 1-8
- Puccinelli A. 1991. Nuovi aspetti dell'evoluzione paleogeografica e tettonica al Plio-Quaternario della Piana di Lucca – New aspects of the paleogeographic and tectonic evolution of the plain of Lucca during Pliocene and Quaternary (Tuscany). *Geografia Fisica e Dinamica Quaternaria* **14**: 171-177.
- Seghieri M. 2006. Pozzeveri. Una Badia, Altopascio, Lucca.
- Soldovieri F., Orlando L. 2009. Novel tomographic based approach and processing strategies for GPR measurements using multifrequency antennas. *Journal of Cultural Heritage* **10S**: 83-92.
- Tinelli C., Ribolini A., Bianucci G., Bini M., Landini W. 2012. Ground penetrating radar and palaeontology: The detection of sirenian fossil bones under a sunflower field in Tuscany (Italy). *Comptes Rendus Paleovol* **11**: 445-454.
- Van Dam R., Schlager W. 2000. Identifying causes of ground-penetrating radar reflections using time-domain reflectometry and sedimentological analyses. *Sedimentology* **47**: 435-449.

Caption to figures

Figure 1 – Geographical (a) and lithological sketch maps (b) of the Badia Pozzeveri site. Geological data from Nardi *et al.*, 2007.

Figure 2 – The San Pietro church on the Badia Pozzeveri site (a, b). Historical map (18th century) showing the position of the site near Lake Sesto (c).

Figure 3 – The four sectors of ground-penetrating radar data capture. Sector 1 is partly overlapped onto the sector surveyed by the STREAM X 200 device (in green).

Figure 4 – Principal outcomes from the archaeological excavation. The limits of GPR surveyed sectors are reported, along with the trace of the GPR profiles discussed in the text.

Figure 5 – The types of GPR reflection in correspondence to a wall. Top and base of the wall reflections (a, c, e) and the effect of coarse boulders composing the later sides of the wall and internal heterogeneity (c, e). The traces of vertical radargrams onto the excavation wall are reported (b, d, f).

Figure 6 – The types of GPR reflection in correspondence to the graves. Reflections from the grave top and base layers (a), horizon lateral truncations feature and chaotic reflections generated by internal material (b). one axis point source hyperbolic reflections and chaotic reflections as generated by rock slab-sided and partly infilled grave (d). The traces of the GPR profile onto excavated graves are reported (c), along with examples of grave infilling (e, f).

Figure 7 - The types of GPR reflections in correspondence to trenches/depressions. Reflections from trench infilling sediments (concave upward reflectors), trench sides (point source hyperbolic reflections) and trench basal gravel (strong flat reflectors) (a). The excavated trench crossed by the L84 GPR profile (a) is evident in (b). Reflections generated by sediments unconformably resting on the base of a pit-kiln (c, d, e, f).

Figure 8 - GPR profile crossing sector 3 (see Figure 4 for location). The principal reflectors with stratigraphical and pedostratigraphical relevance are traced with fine discontinuous and dotted lines. Thick discontinuous lines indicate the trace of truncation surfaces. The positions of possible graves are reported.

Figure 9 – Amplitude maps at different depths (a, b) of sector 1. Position of the sector in the churchyard is reported (c). The meaning of the letters on the amplitude maps is discussed in the text.

Figure 10 – Amplitude map at different depths (a, b) of sector 2. Position of the sector in the churchyard is reported (c). The meaning of the letters on the amplitude maps is discussed in the text.

Figure 11 – Amplitude maps at different depths (a, b) of sector 3. Position of the sector in the churchyard is reported (c). The meaning of the letters on the amplitude maps is discussed in the text.

Figure 12 – Amplitude maps at different depths (a, b) of sector 4. Position of the sector in the churchyard is reported (c). The meaning of the letters on the amplitude map is discussed in the text.

1
2
3
4
5
6
7
8
9
10
11
12
13
14
15
16
17
18
19
20
21
22
23
24
25
26
27
28
29
30
31
32
33
34
35
36
37
38
39
40
41
42
43
44
45
46
47
48
49
50
51
52
53
54
55
56
57
58
59
60

612 Figure 13 – Comparison between STREAM X 200 MHz and 400 MHz amplitude maps.
613 See Figure 3 for area location overlap. The meaning of the letters on the amplitude
614 maps is discussed in the text.

For Peer Review Only

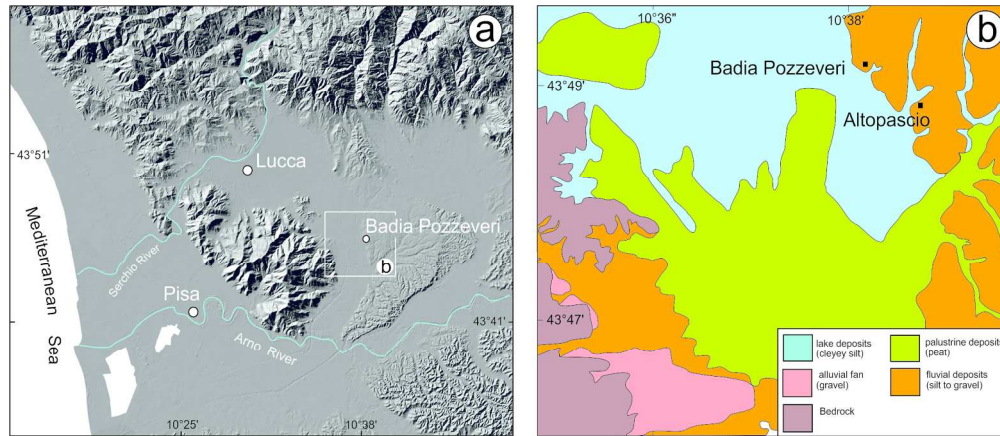
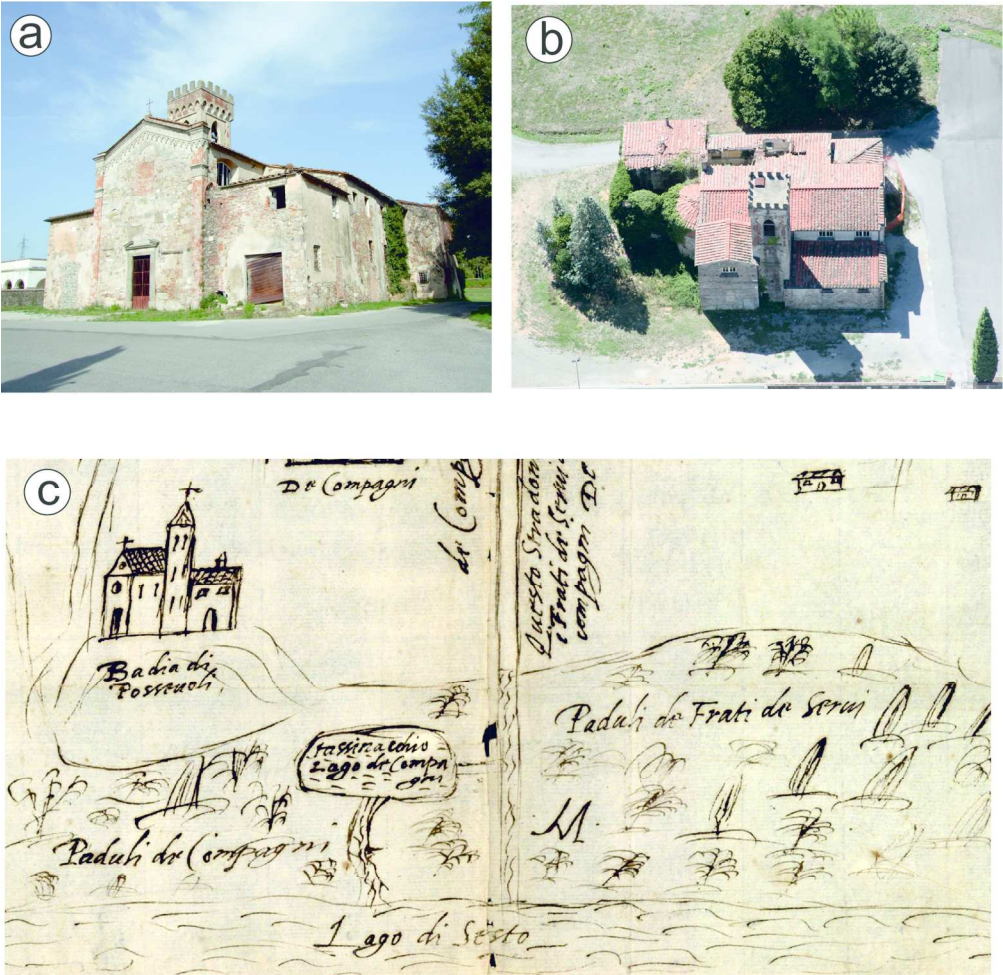


Figure 1

188x81mm (300 x 300 DPI)

1
2
3
4
5
6
7
8
9
10
11
12
13
14
15
16
17
18
19
20
21
22
23
24
25
26
27
28
29
30
31
32
33
34
35
36
37
38
39
40
41
42
43
44
45
46
47
48
49
50
51
52
53
54
55
56
57
58
59
60



154x149mm (300 x 300 DPI)

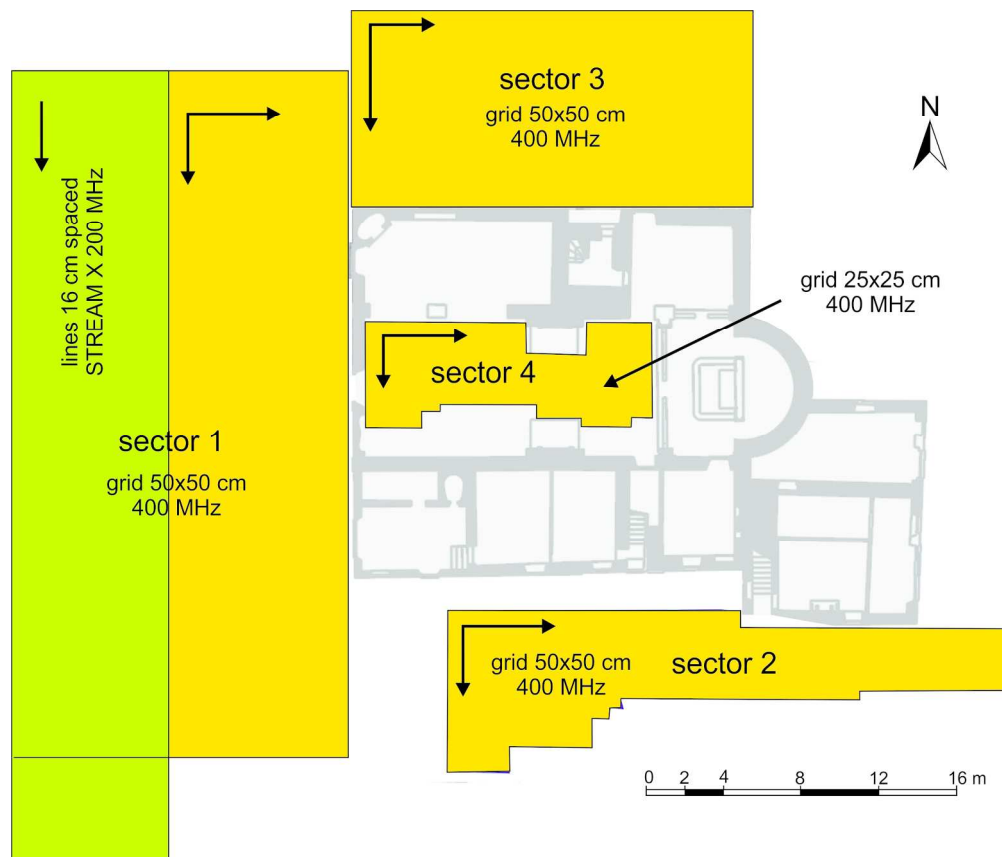


Figure 3

181x154mm (300 x 300 DPI)

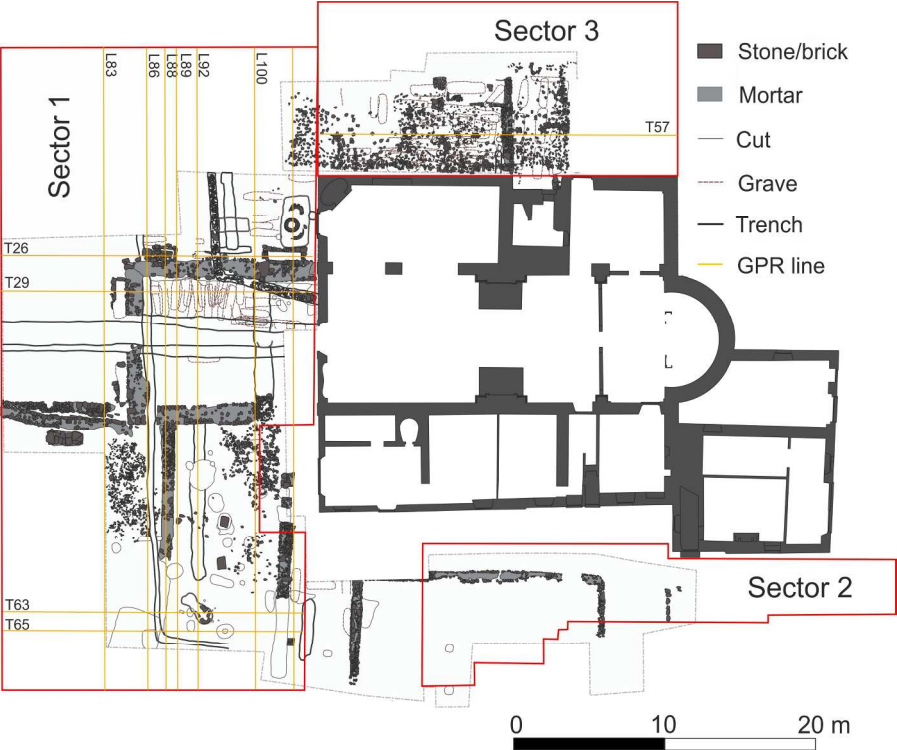


Figure 4

225x168mm (300 x 300 DPI)

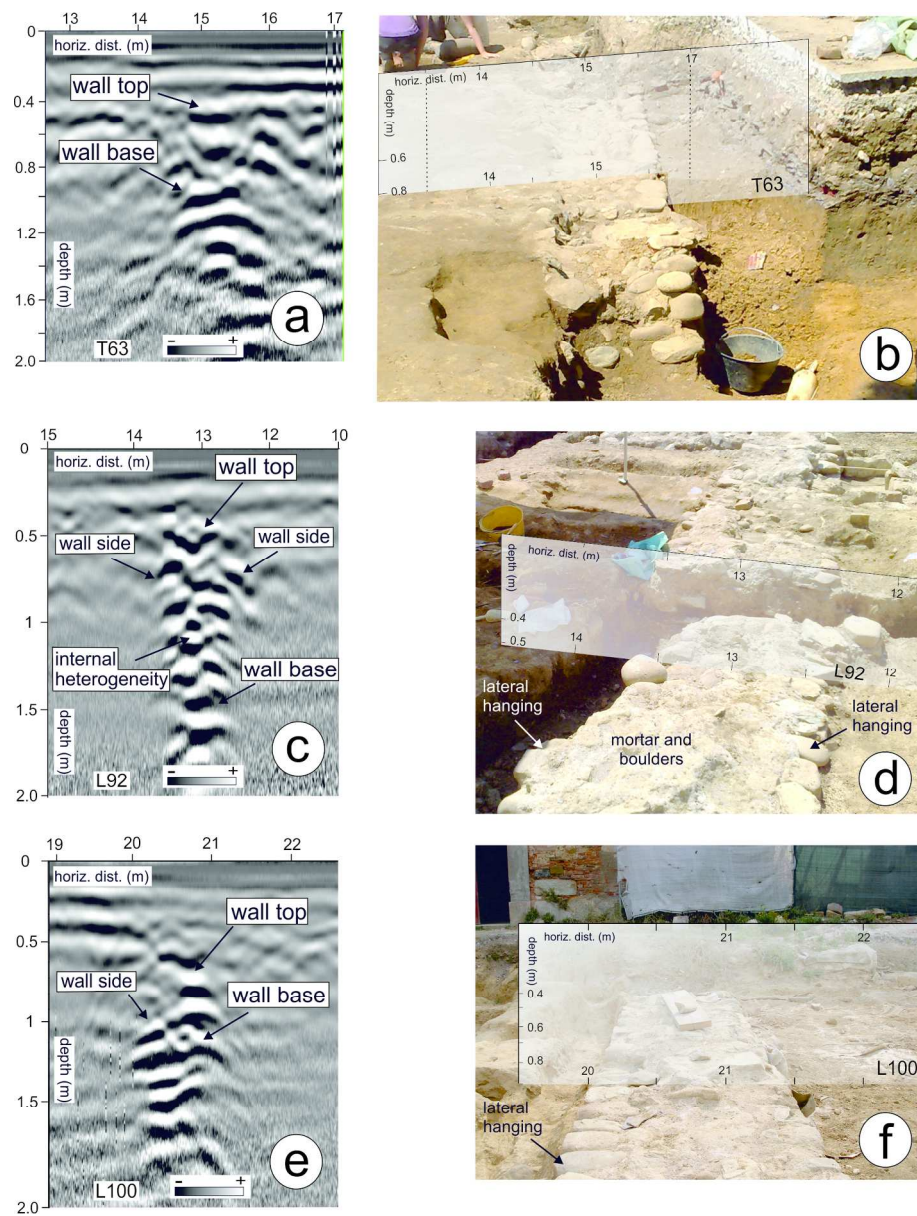


figure 5

180x228mm (300 x 300 DPI)

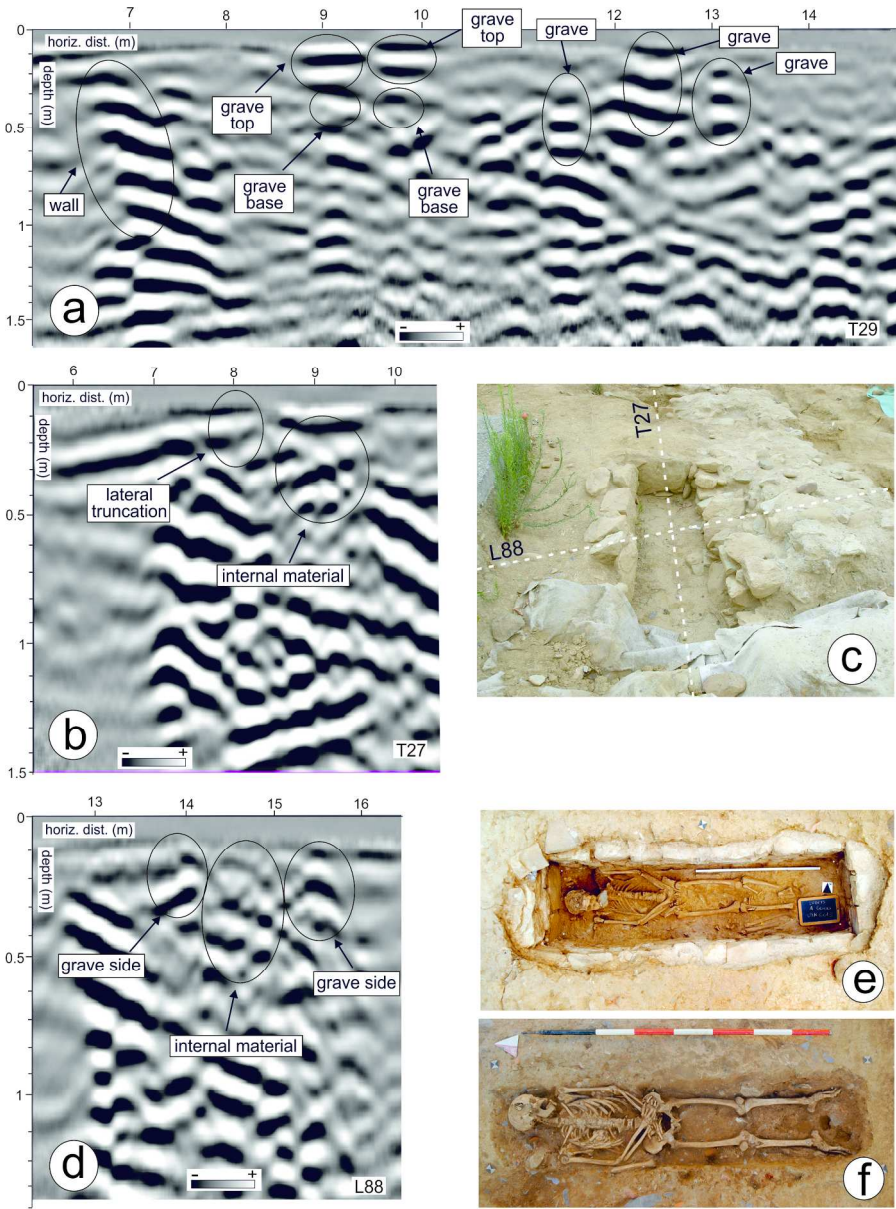


Figure 6

183x246mm (300 x 300 DPI)

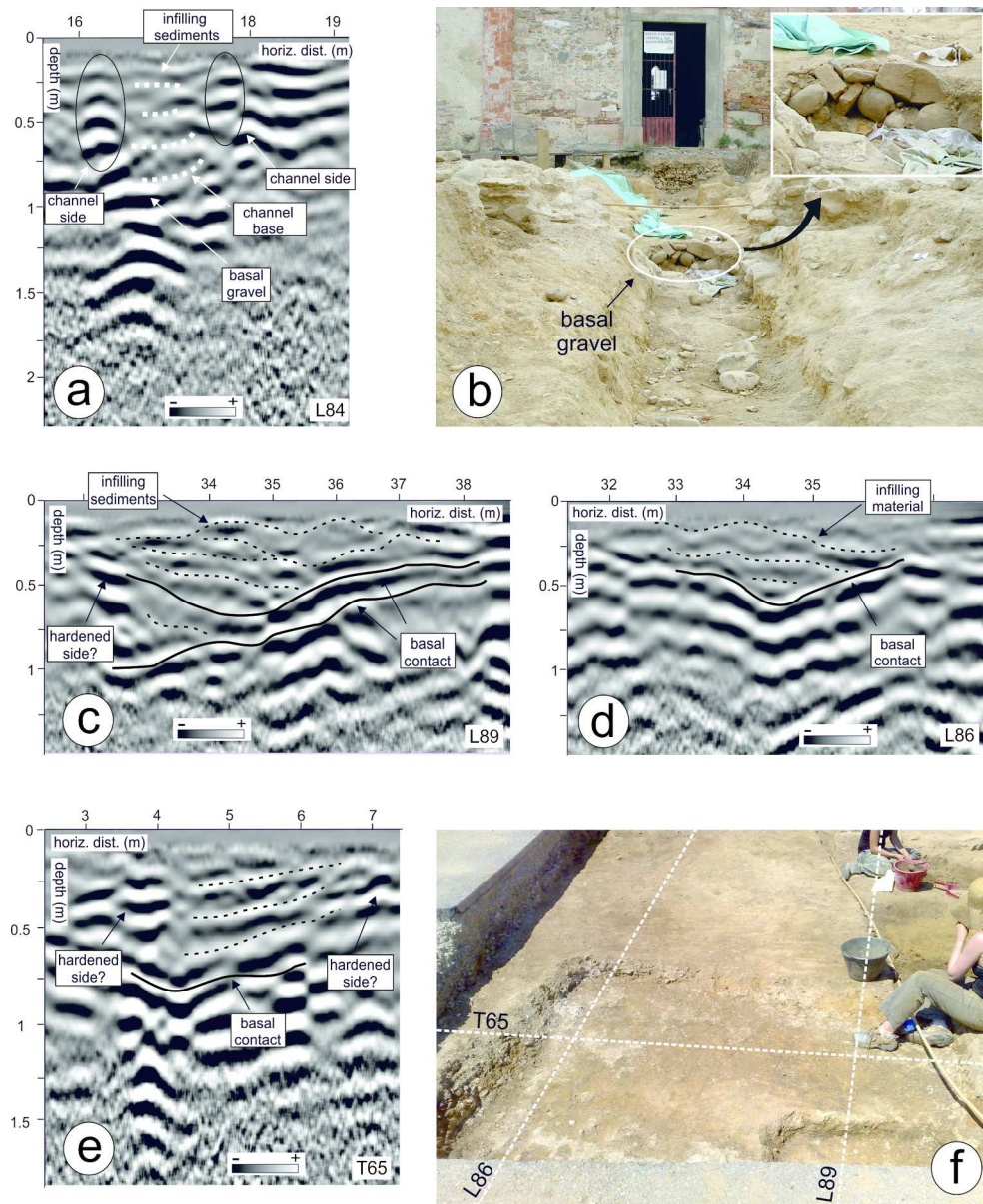


Figure 7

193x236mm (300 x 300 DPI)

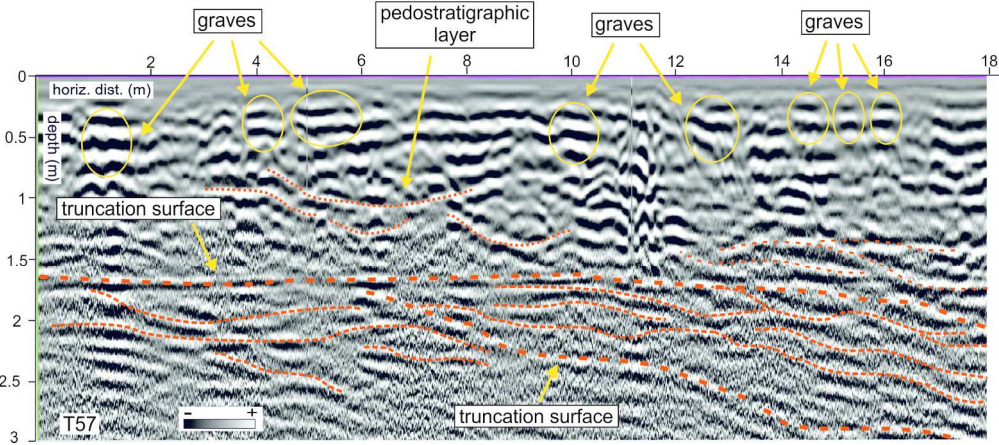


Figure 8

183x80mm (300 x 300 DPI)

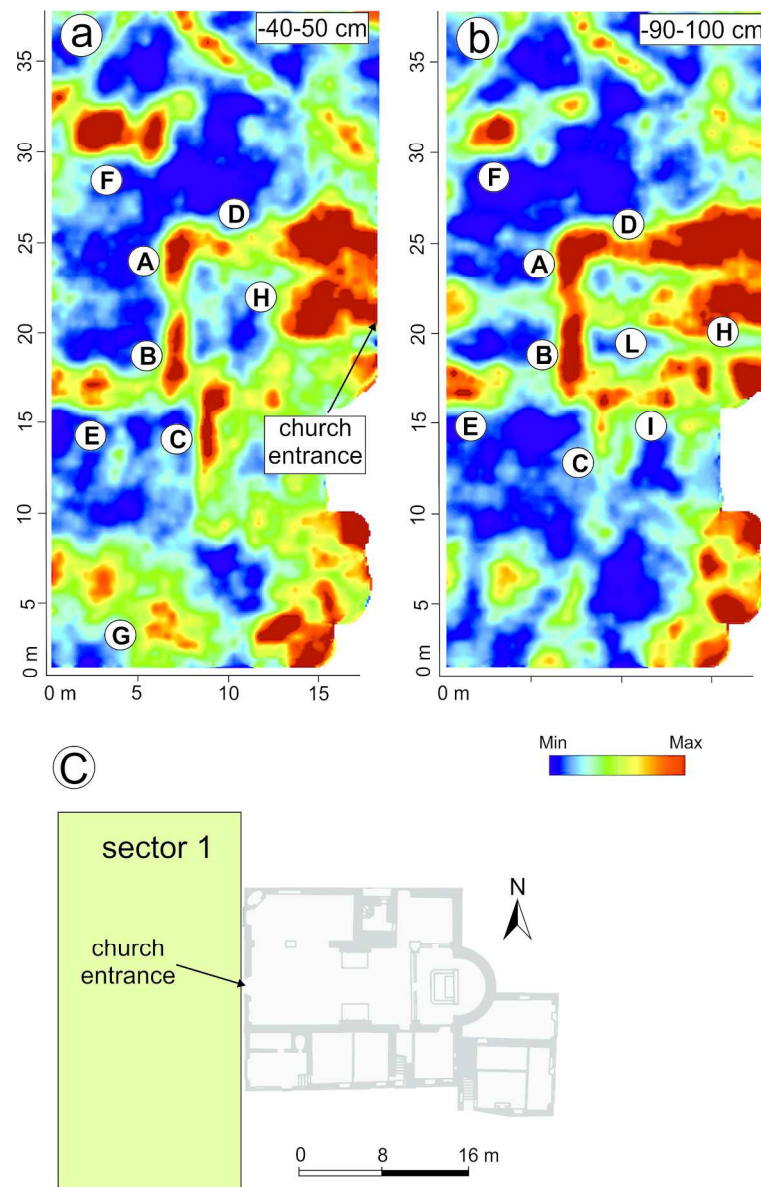


Figure 9

153x243mm (300 x 300 DPI)

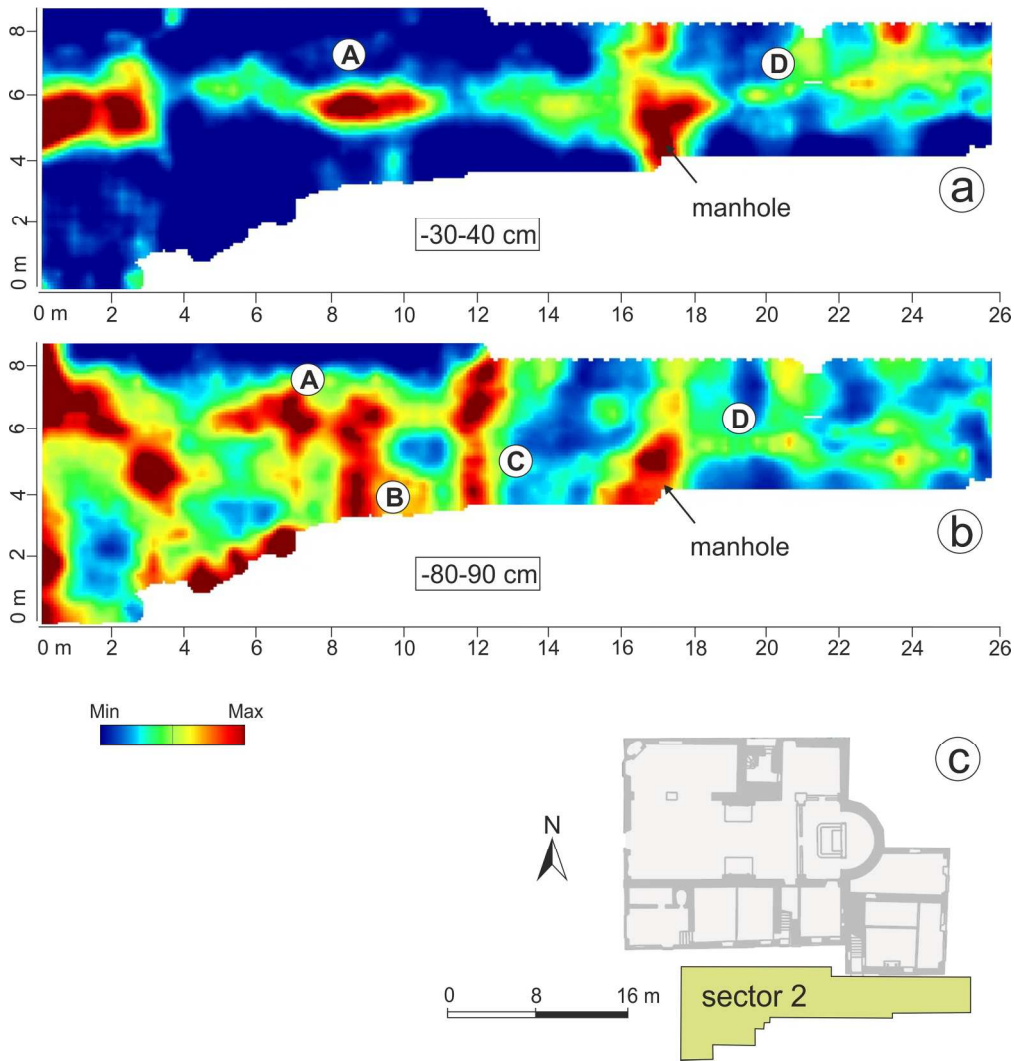


Figure 10

191x201mm (300 x 300 DPI)

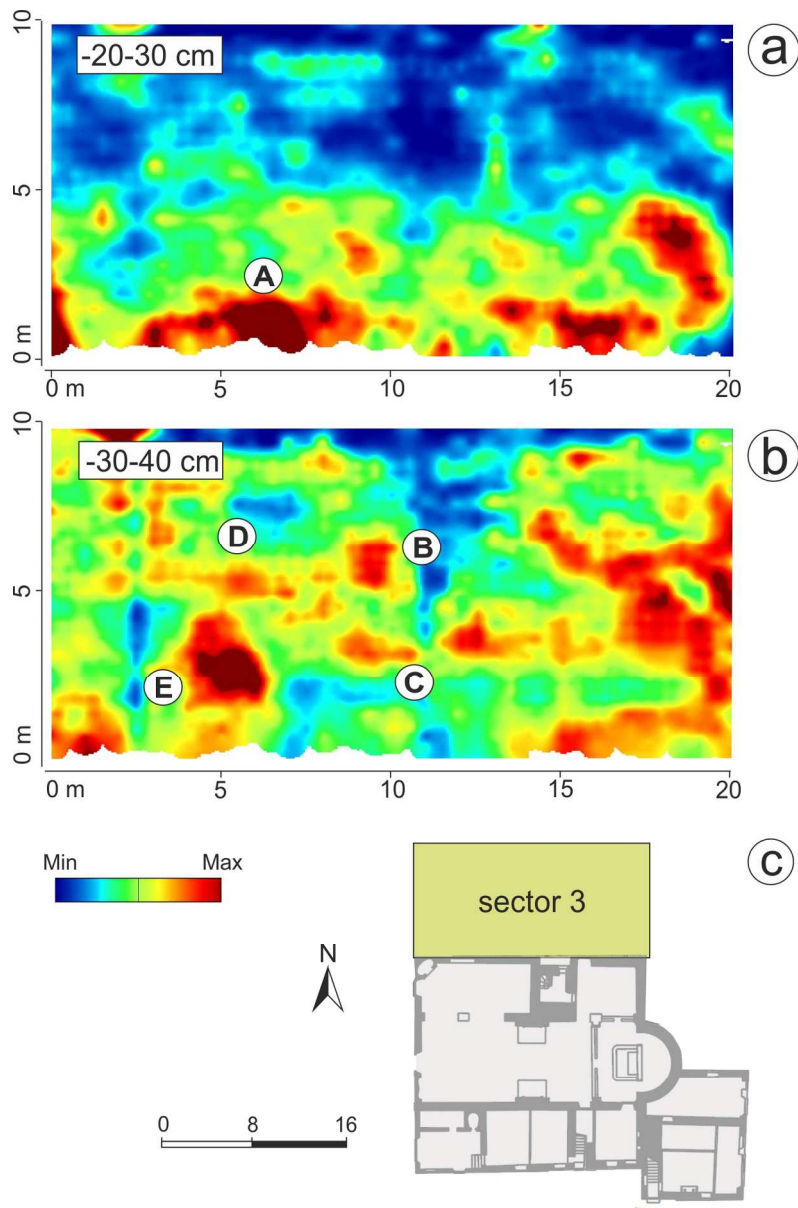


Figure 11

130x199mm (300 x 300 DPI)

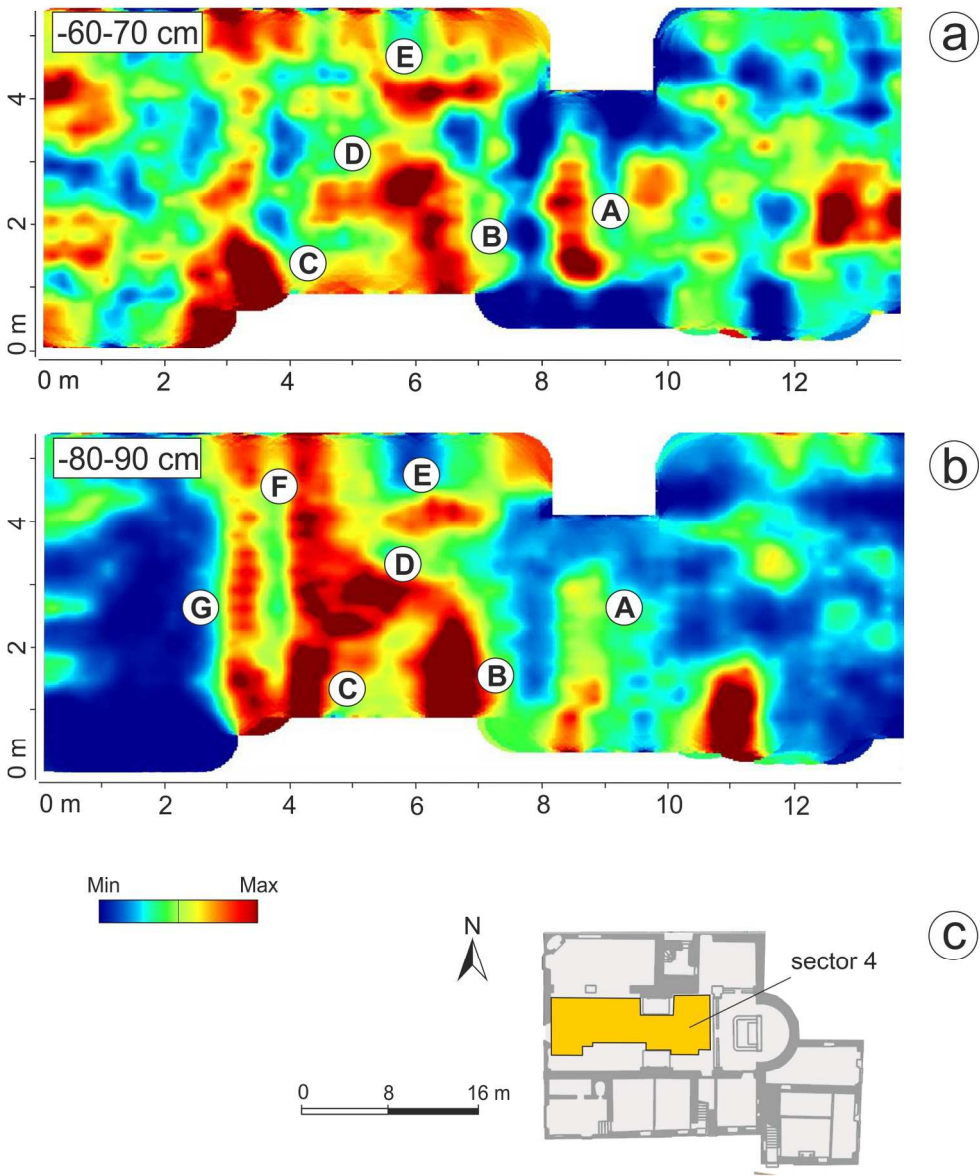


Figure 12

168x209mm (300 x 300 DPI)

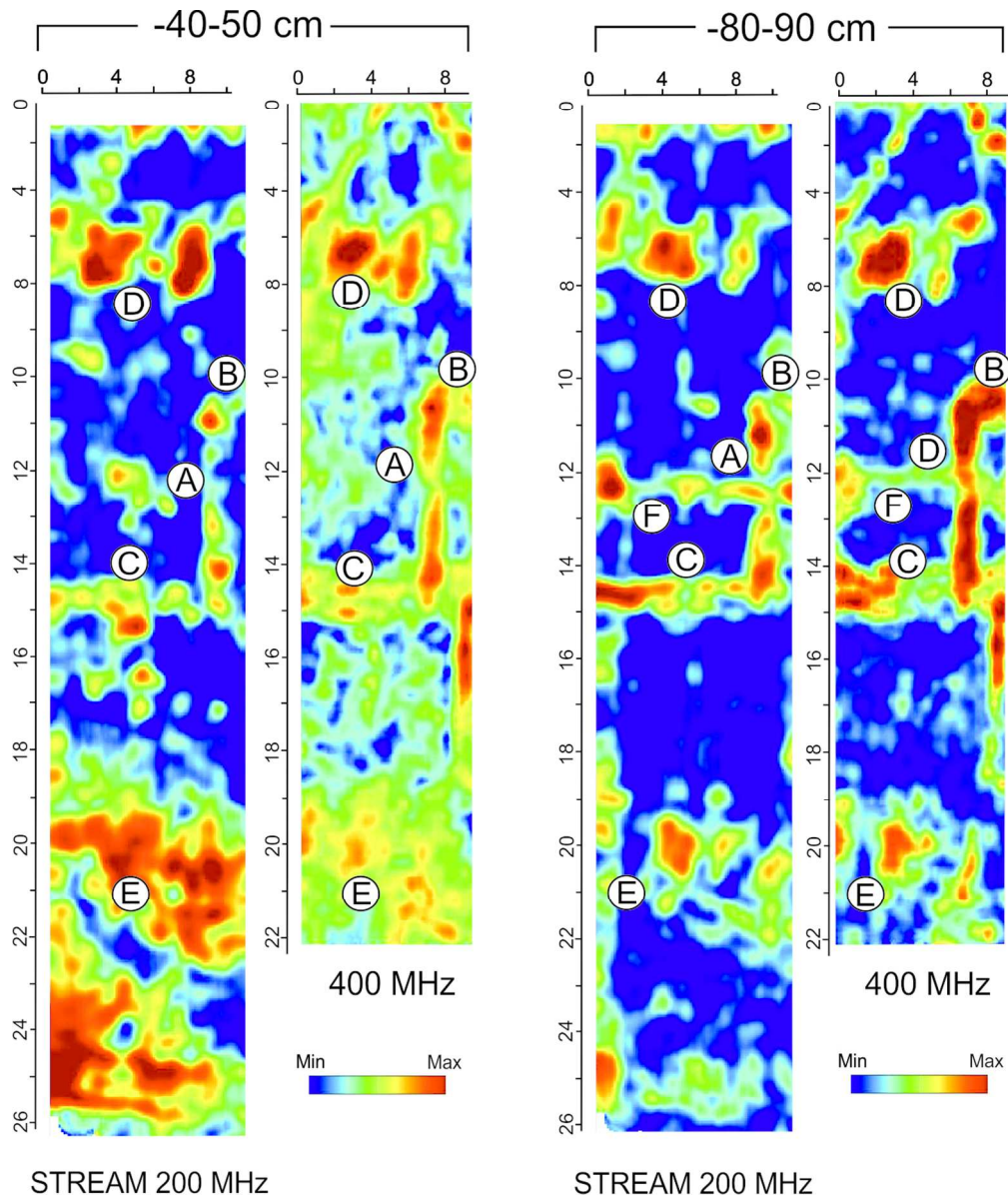


Figure 13

112x133mm (300 x 300 DPI)